Unconventional behavior of the Ce3Pt23Si11 ferromagnet

Christine Opagiste, Rose-Marie Galéra, Mehdi Amara, Carley Paulsen, S. Rols, B. Ouladdiaf

Unconventional behavior of the $Ce_3Pt_{23}Si_{11}$ ferromagnet

C. Opagiste,[1,*] R.-M. Galéra,[1] M. Amara,[1] C. Paulsen,[1] S. Rols,[2] and B. Ouladdiaf[2]

[1] *Institut Néel, CNRS-UJF, BP 166, F-38042 Grenoble Cedex 9, France*

[2] *Institut Laue-Langevin, 6 rue Jules Horowitz, BP 156, 38042 Grenoble Cedex 9, France*

(Dated: October 14, 2011)

It was recently demonstrated on high quality single crystal that $Ce_3Pt_{23}Si_{11}$ orders ferromagnetically at $T_C = 440$ mK. Extensive studies of the physical properties of this compound are reported. In the paramagnetic phase, heat capacity and electrical resistivity measurements on a single crystal confirm a good metal behavior with a residual resistivity of $\rho_0 = 12.17$ $\mu\Omega$ cm, no Kondo-type anomaly and a Debye temperature of 280 K, similar to the one of the the iso-structural non-magnetic compound $La_3Pt_{23}Si_{11}$. In the ferromagnetic phase, the easy magnetization axis is the threefold one with a spontaneous magnetization of 0.91 μ_B/Ce at 100 mK. This value differs from the expectations within a cubic crystalline electric field (CEF) model. More surprisingly, the inelastic neutron scattering shows two CEF peaks while neutron diffraction experiments reveals that the structure remains cubic down to 800 mK. These results are very reminiscent of those of $CeAl_2$. Using the CEF formalism, the fits of the magnetic susceptibility lead to a quadruplet ground state which is not consistent with the anisotropy found in the ferromagnetic state. This strongly suggests a splitting of the ground state by a dynamical Jahn-Teller effect which retains the apparent cubic symmetry for static measurements.

PACS numbers: 75.25.-j, 75.30.Cr, 75.10.Dg, 75.50.Cc
Keywords: ferromagnetism, cerium intermetallic compounds, crystal electric field, neutrons diffraction, neutrons scattering

I. INTRODUCTION

In the search of new cerium heavy fermion compounds, the ternary Ce-Pt-Si phase diagram has been the focus of great interest and generated extensive investigations. The existence of a new compound defined as $Ce_3Pt_{23}Si_{11}$ was first reported by Tursina et *al.* who have determined the crystal structure, $Fm\bar{3}m$.[1] An isothermal cross-section of the Ce-Pt-Si phase diagram have shown that $Ce_3Pt_{23}Si_{11}$ is in equilibrium with the non-centrosymetric heavy fermion superconductor $CePt_3Si$, when this last compound is deficient in cerium composition.[2] $CePt_3Si$ orders antiferromagnetically at $T_N = 2.2$ K and presents a heavy fermion superconducting state at $T_c = 750$ mK. Many studies on the superconductivity of $CePt_3Si$ reveal an extra transition around 500 mK.[3–5] Only very few studies on the role of structural defects and of impurity effects have been reported.[6,7] It still leaves the question open whether the transition around 500 mK is intrinsic to the $CePt_3Si$ phase or due to an impurity phase. $Ce_3Pt_{23}Si_{11}$, which was first reported to order antiferromagnetically at very low temperatures, was suspected to interfere with the $CePt_3Si$ physical properties.[5] Indeed small amounts of $Ce_3Pt_{23}Si_{11}$ could easily be present in $CePt_3Si$ samples. It is therefore essential to have a better understanding of the physical properties of this new $Ce_3Pt_{23}Si_{11}$ compound.

Our recent studies on a very high quality single crystal of $Ce_3Pt_{23}Si_{11}$ reveal a ferromagnetic transition at $T_c = 0.44$ K. Below T_c, a power law scaling fit of the spontaneous magnetization vs. $(T\text{-}Tc)^{\beta}$ gives a value of 1.1 μ_B/Ce for Ms(0), the magnetic saturation moment extrapolated to 0 K.[8] This low value, compared to the theoretical one of 2.14 μ_B/Ce, is ascribed to the CEF effects.

We report here extensive studies of bulk physical properties of $Ce_3Pt_{23}Si_{11}$ and its non magnetic counter part $La_3Pt_{23}Si_{11}$ together with studies at the microscopic scale using neutrons scattering in order to get deeper insight into the cerium behavior in $Ce_3Pt_{23}Si_{11}$. In this paper, the crystallographic properties of the samples are presented in section II. The thermodynamic and the transport properties are analyzed in section III. Section IV contains the magnetization measurements and is followed by the neutron studies, spectroscopy in the paramagnetic phase and diffraction in the ferromagnetic state (section V). The last section is devoted to the discussion about experimental results.

II. SAMPLE ELABORATION AND CRYSTALLOGRAPHIC ANALYSIS

High quality polycrystalline samples of $Ce_3Pt_{23}Si_{11}$ and $La_3Pt_{23}Si_{11}$ have been prepared in an induction furnace. Stoichiometric proportions of the different constituents: Ce or La (99.99%, Johnson Matthey), Pt (99.95%, Alfa Aesar) and Si (99.9999%, Alfa Aesar), were melted in a cold copper crucible under a high purity argon atmosphere. Samples were melted several times to improve the homogeneity. Mass losses during this first step were less than 0.1%. The sample quality was checked by conventional X-ray powder diffraction (Cu-Kα radiation on a Philipps PW1730 diffractometer). $Ce_3Pt_{23}Si_{11}$ and $La_3Pt_{23}Si_{11}$ crystallize in the same face-centered cubic structure of the $Fm\bar{3}m$ space group, Ce^{3+} and La^{3+} ions

are located on the *24d* sites. Within the experimental accuracy, no impurity phases are detected. The values of the refined lattice parameter are $a_{La} = 16.8953(2)$ Å and $a_{Ce} = 16.8747(2)$ Å for $La_3Pt_{23}Si_{11}$ and $Ce_3Pt_{23}Si_{11}$ respectively. These values are consistent with the volume contraction in the lanthanide series.

From the polycrystalline batch of $Ce_3Pt_{23}Si_{11}$ a single crystal was grown using the Czochralski technique.[8] Samples of different shapes were cut from the single crystalline $Ce_3Pt_{23}Si_{11}$ ingot: a sphere of $\phi = 2$ mm in diameter for magnetization measurements, a long bar of section $S = 0.1$ mm^2 and length $\ell_{\|[001]} = 1$ mm for resistivity measurements and a truncated cone of sections $S_1 = 0.93$ mm^2, $S_2 = 1.32$ mm^2 and length $\ell = 4.86$ mm for neutron diffraction experiments. All these samples were annealed at 900°C for 7 days in an ultra high vacuum furnace in order to relax the internal stresses. The single crystalline samples were oriented using the back scattering X-ray Laue diffraction technique on a PANanalytical PW3830 diffractometer.

III. THERMODYNAMIC AND TRANSPORT PROPERTIES

The heat capacity and the electrical resistivity were measured in the temperature range 0.38 - 300 K using a Quantum Design-Physical Property Measurement System (QD-PPMS). The measurement of the heat capacity is based on the relaxation method. Samples are glued with Apiezon N grease in order to be thermally coupled to the puck platform. As both $Ce_3Pt_{23}Si_{11}$ and $La_3Pt_{23}Si_{11}$ compounds are good metals they reveal a weak heat capacity, even weaker than the addenda contribution. Therefore, to obtain the experimental curves with the best accuracy, we used the following procedure: a first measurement is made with the empty puck and the grease and then a second measurement is performed after having deposited the sample on the previous setup. The heat capacity of the sample is then obtained by subtracting the puck+Apiezon signal from the total heat capacity measured with the sample. For electrical resistivity measurements a 4-probe method was used. For $Ce_3Pt_{23}Si_{11}$, the single crystalline bar was used with a low current excitation of 1 mA along the [001] crystallographic direction.

In the considered temperature range, the heat capacity of a rare earth-based metallic material can be given by $C = C_{el} + C_{ph} + C_{mag} + C_{CEF}$. The first two terms represent the purely lattice contribution, $C_{el} = \gamma$T is the contribution of the conduction electrons and C_{ph} the phonon contribution, which can be expressed in the Debye model as:

$$C_{ph} = 9nR\left(\frac{T}{\theta_D}\right)^3 \int_0^{\theta_D/T} dx \frac{x^4 e^x}{(e^x-1)^2} \qquad (1)$$

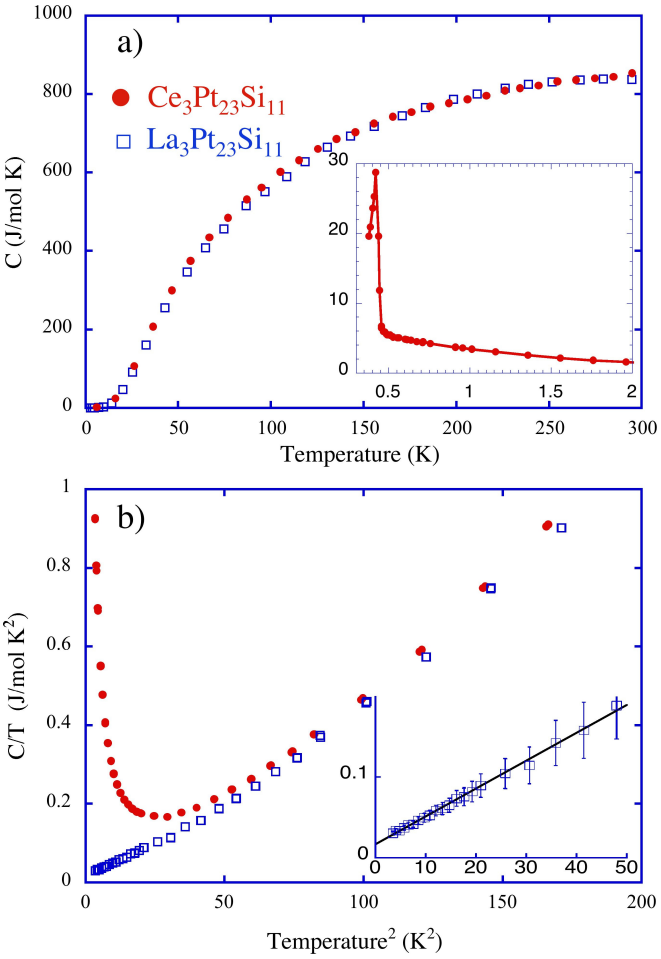

FIG. 1. (Color online) a) Thermal variation of the specific heat of $Ce_3Pt_{23}Si_{11}$ (full dots) and $La_3Pt_{23}Si_{11}$ (open squares). The inset shows the low temperature data with a large anomaly at the ferromagnetic transition ($T_C = 440$ mK). b) C/T vs. T^2 for the same samples. For the non-magnetic compound $La_3Pt_{23}Si_{11}$ the Debye temperature and the electronic coefficient are deduced from the linear fit shown in the inset (solid line): $\theta_D = 280 \pm 3$ K and $\gamma = 18.4 \pm 1.7$ mJ/mol K^2.

n is the number of atoms per formula unit (here $n = 37$), R the molar gas constant and θ_D the Debye temperature. C_{ph} tends asymptotically to $3nR$ for T >> θ_D (the Dulong and Petit law) while for T << θ_D, $C_{ph} \approx \frac{12\pi^4}{5} nR \left(\frac{T}{\theta_D}\right)^3$.

The crystalline electric field, C_{CEF}, contribution has the following expression:

$$C_{CEF} = \frac{R}{(k_B T)^2}\left[\sum_{i,k} p_i E_i^2 - \left(\sum_{i,k} p_i E_i\right)^2\right] \qquad (2)$$

k_B is the Boltzman constant and p_i the Boltzman occupation probabilities of the CEF energy levels E_i. C_{CEF}

accounts for the Schottky anomalies arising from the splitting of the J fundamental multiplet of the rare earth ions by the crystalline electric field.

The contribution due to the purely magnetic ordering, C_{mag} can be deduced from the experimental data by subtracting all the aforesaid contributions. Figure 1-a shows the thermal variation of heat capacity of $Ce_3Pt_{23}Si_{11}$ and $La_3Pt_{23}Si_{11}$. For both compounds the evolution at high temperature of the specific heat appears consistent with the Debye law. At 300 K, C reaches about 91% of the value at saturation $3nR$ *i.e.* 922.89 J/mol K. The inset in figure 2 shows the measurement at low temperature. As in Ref. 9, the heat capacity shows a minimum around 5 K. Below this temperature it starts increasing smoothly down to 0.5 K and then initiates a steep upturn associated to the ferromagnetic transition. The value of T_C is in agreement with the value in Ref. 8. Unfortunately the base temperature of the commercial device (380 m K) is to close to T_C. This hinders the measurement of the whole lambda-anomaly and thus a proper determination of the magnetic entropy.

The curves C/T vs. T^2 at low temperature for the La and Ce compounds are plotted in figure 1-b. For $La_3Pt_{23}Si_{11}$ this evolution becomes linear from T^2 = 45 K^2 down to the lowest reached temperature. A least squares fit with the function $\gamma+\beta T^2$ yields to an electronic coefficient γ = 18.4 ± 1.7 mJ/mol K^2 and a Debye temperature θ_D = 280 ± 3 K. From the experimental curves of the specific heat (see Fig. 1) it is clear that the lattice contributions are similar in the Ce and La compounds. This is confirmed by the value of θ_D = 280 K for $Ce_3Pt_{23}Si_{11}$ deduced from that of $La_3Pt_{23}Si_{11}$ using the procedure in Ref 10. The values of θ_D and γ are fully consistent with those reported in Ref. 9. The comparison of the heat capacity between the Ce and the La compounds in the whole explored temperature range (see Fig. 1) strongly supposes a negligible CEF contribution. Calculations of this contribution using the different CEF diagrams compatible with the neutron scattering results (section V) have confirmed this observation.

The electrical resistivity of both the $Ce_3Pt_{23}Si_{11}$ and the $La_3Pt_{23}Si_{11}$ samples is characteristic of a good metal (see Fig. 2). The ratio $\rho_{300K}/\rho_{1.8K}$ for the La sample ($\approx$ 3.25) is twice lower than that for the Ce sample ($\approx$ 6.75). This is due to the fact that the La sample is a polycrystal. Therefore the magnetic resistivity cannot be determined by simply subtracting the La resistivity from the Ce one. Nonetheless the residual resistivity ($\rho_0 \approx 26.3$ $\mu\Omega$ cm) of the La sample is four times smaller than the value reported in Ref. 9. The comparative study of the specific heat and electrical resistivity, between the lanthanum and cerium compounds, proves that the cerium compound is neither a Kondo nor an intermediate valence system.

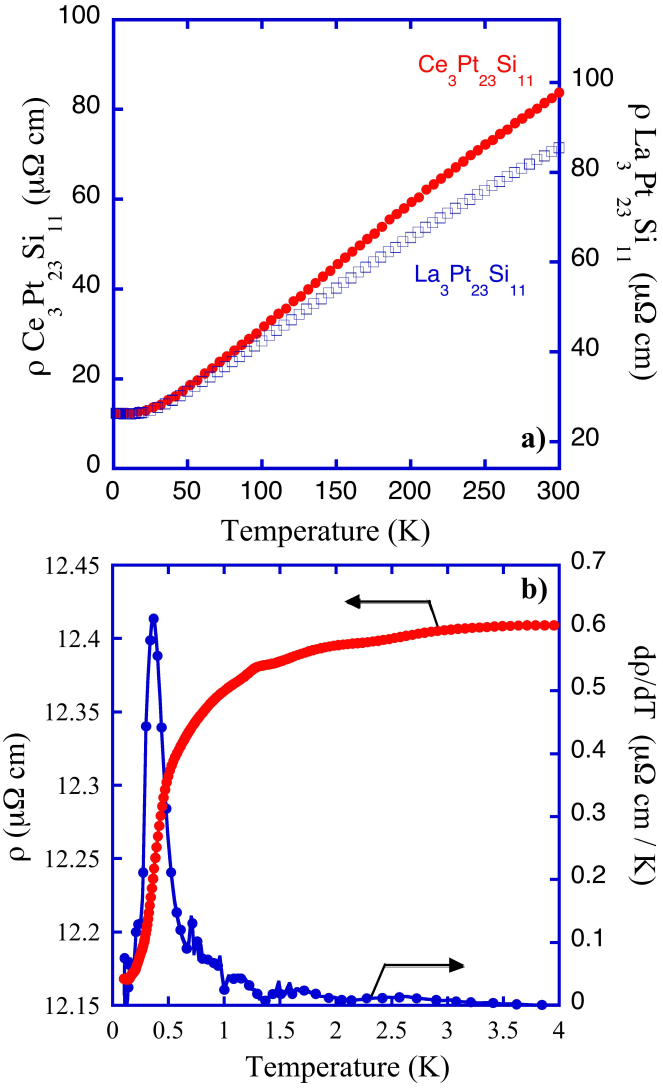

FIG. 2. (Color online) a) Electrical resistivity of the single crystalline sample of $Ce_3Pt_{23}Si_{11}$ and of a polycrystalline sample of $La_3Pt_{23}Si_{11}$ over 300 K - 1.8 K. b) Electrical resistivity of the single crystalline sample of $Ce_3Pt_{23}Si_{11}$ in the temperature range 100 mK - 4 K. The ferromagnetic transition at 440 mK is indicated by the peak in the temperature derivative dρ/dT.

IV. MAGNETIC PROPERTIES

Magnetization measurements were performed at the Néel Institute using different magnetometers based on the extraction method. From room temperature down to 1.9 K, the measurement of the magnetization M(T) was carried out using a commercial Quantum Design Magnetic Property Measurement System (MPMS) magnetometer. The absolute sensitivity is 10^{-11} A m^2 at 0.25 Tesla and the accuracy is 0.1% for a cylindrical standard sample (ϕ = 3 mm, h = 3 mm). Measurements were performed using the reciprocating sample option (RSO) under an applied field of 1 T. The signal was

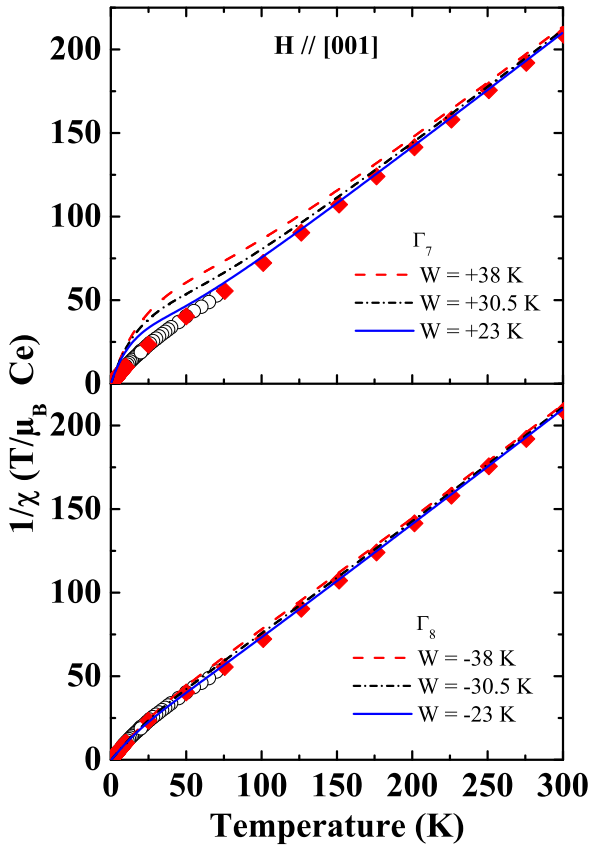

FIG. 3. (Color online) Thermal variation of the inverse of the magnetic susceptibility for an applied field along the [001] symmetry axis of the crystal. Full diamonds represent the susceptibility deduced from the thermal variation of the magnetization in a field of 0.1 T measured using the QD SQUID. Open circles represent the susceptibility deduced from the Arrott plots. The lines represent the calculated curves using the values of the CEF parameter W reported in the figure.

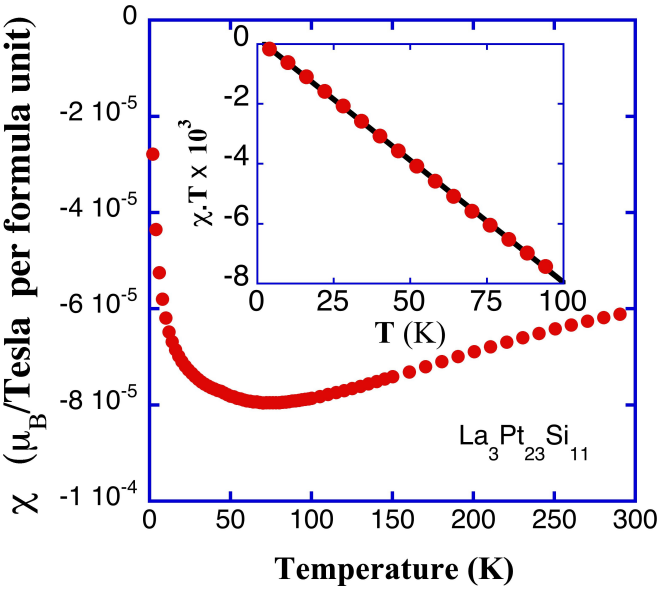

FIG. 4. (Color online) Thermal variation of the susceptibility of $La_3Pt_{23}Si_{11}$. The upturn at low temperatures can be ascribed to a weak amount of paramagnetic impurities in the diamagnetic matrix. The inset shows the curve χ T = f(T). From the linear fit (black line), and assuming a contamination by iron impurities (α-Fe, m = 2.2μ_B) one could estimate that the upturn corresponds to 1.7 ppm.

recorded with the sample oscillating around the center of the SQUID pick up coils and fitted to an ideal dipole response using a non-linear least-squares routine. The M(T) curves have been measured on a polycrystalline sample of $La_3Pt_{23}Si_{11}$ and on the single crystalline sphere of $Ce_3Pt_{23}Si_{11}$. For $Ce_3Pt_{23}Si_{11}$ the field was applied successively along the [001] and [111] high symmetry axes of the cubic structure. For both compounds the susceptibility is given by χ(T) = M(T)/H.

For $Ce_3Pt_{23}Si_{11}$, magnetization curves M(H) have been performed in the temperature range 2-75 K using a in-house experimental setup that allows precise measurements on oriented single crystals. The cryomagnet can supply magnetic field up to ±10.5 T and the sensitivity of the measurement reaches 10^{-7} A m^2 in the temperature range 1.5 - 300 K. The magnetization processes have been measured up to 8 T applied along the [001] axis. The inverse of the magnetic susceptibility is deduced from the Arrott plots[11]: M^2 = f(H/M), at the intercept between the linear part of the Arrott plot and the x axis.

The thermal variation of magnetic susceptibility deduced from the present measurements reveals no anisotropy between the [001] and [111] axes as expected for a cubic symmetry. For clarity, only the measurements along the fourfold axis have been reported in figure 3 of the inverse of the susceptibility, $1/\chi$. The results confirm a Curie-Weiss-type behavior from room temperature down about 100 K. A linear fit in this temperature range gives an experimental Curie constant of 1.47 μ_B K/T in fairly good agreement with the theoretical value of 1.44 μ_B K/T. Below 100 K $1/\chi$ deviates from the Curie-Weiss law and shows a downward curvature. In rare earth based compounds this deviation is usually ascribed to the crystalline electric field (CEF) effects. The $4f$ orbitals are coupled with the electric charges surrounding the rare earth ions and this interaction partly or totally removes the degeneracy of the ground state multiplet J. For Ce^{3+} ions in a cubic symmetry, the CEF splits the 6 levels of the $J = 5/2$ ground state multiplet into a Γ_7 doublet and a Γ_8 quadruplet. This leads to a reduction of the moment at low temperatures. Thus, for a fully degenerate $J = 5/2$ ground state, the moment at 0 K is $\mu_s(0\ \mathrm{K}) = g_J J = 2.14\ \mu_B/Ce$. For the isolated Γ_7 and Γ_8 ground states its value is $\mu_s(0\ \mathrm{K}) = 0.714\ \mu_B/Ce$ and $\mu_s(0\ \mathrm{K}) = 1.571\ \mu_B/Ce$ respectively.

The magnetic susceptibility of $La_3Pt_{23}Si_{11}$ shows a

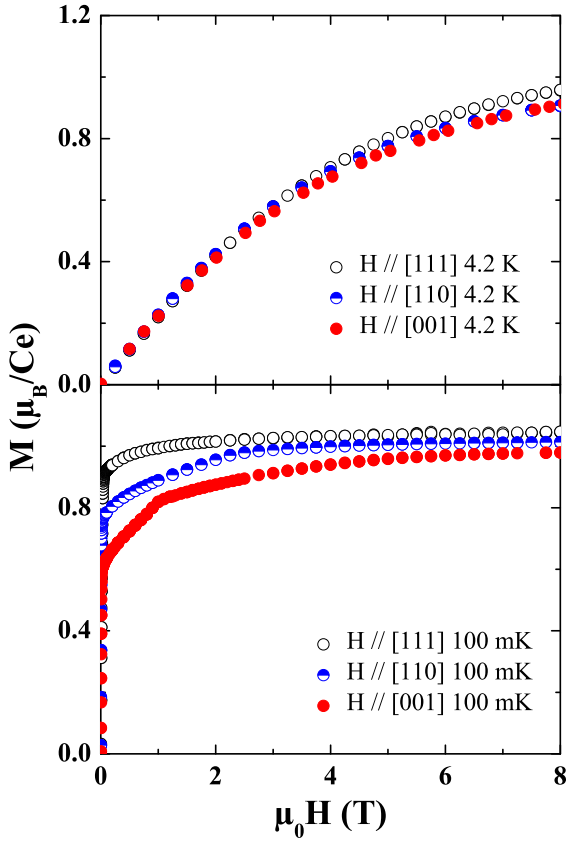

FIG. 5. (Color online) Magnetization curves measured with the field applied successively along the three main axes of the cube. Bottom part shows the measurements in the ferromagnetic phase at 100 mK and upper part measurements at 4.2 K. The [111] direction is clearly the easy magnetization axis.

diamagnetic behavior with a slight upturn below 50 K, characteristic of a weak amount of paramagnetic impurities (see figure 4). From the linear fit of the curve $\chi\ T = f(T)$ (see inset fig. 4) an effective Curie constant value of 1.76 $10^{-4}\mu_B$ K/T per formula unit is deduced. Assuming a contamination by iron impurities (α-Fe, $m = 2.2\ \mu_B$) one could estimate that the upturn corresponds to 1.7 ppm. This estimation is consistent with the certificate analysis of the initial components.

In order to study the ferromagnetic transition, a series of measurements were made using the high field SQUID magnetometers developed at the Néel Institute. It is equipped with a miniature dilution refrigerator that can cool the sample below 100 mK, and it has a superconducting magnet for fields up to ± 8 T. A unique feature of the setup is that absolute values of the susceptibility and magnetization can be made by the extraction method at very low temperatures. The experimental sensitivity is also of the order of 10^{-11}A m^2. Figure 5 shows the magnetization curves measured at 4.2 K and in the ferromagnetic phase, at 100 mK, along the three main axes of the cube. In the ordered phase the easy magnetization axis is obviously the threefold [111] axis. At low fields, the spontaneous magnetization M_s(T) at 100 mK is deduced from the Arrott plots of the experimental curves. $M_{s//[111]} = 0.91\pm0.02\ \mu_B/Ce$. This value is in rather good agreement with that previously deduced from the power law scaling expression.[8] Increasing the field, the magnetization rapidly saturates to the value $M_{sat} = 1.05\pm0.02\ \mu_B/Ce$. $M_{s//[110]} = 0.76\pm0.02\ \mu_B/Ce$ and $M_{s//[001]} = 0.59\pm0.02\ \mu_B/Ce$ along the [110] and [001] axes respectively. These values compare rather well with $\sqrt{\frac{2}{3}}M_{s//[111]} = 0.74\ \mu_B/Ce$ and $\frac{1}{\sqrt{3}}M_{s//[111]} = 0.53\ \mu_B/Ce$ expected from the Néel phase law. Along the [110] axis the curve is in agreement with the theoretical magnetization processes. When the applied field has purified the domains and the magnetization has reached its spontaneous value, the magnetic moment of each atom starts to rotate against the local anisotropy with increasing the field until it becomes parallel to the field direction (here around 3 T) and then, the magnetization saturates at M_{sat}= $1.02\pm0.02\ \mu_B/Ce$. Along the [001] axis the saturation of the magnetization is reached in fields larger than 5 T, $M_{sat} = 0.98\pm0.02\ \mu_B/Ce$. Along this direction a small kink is observed around 1 T. The origin of this kink is not understood yet, but it was carefully checked that it is not an artifact due, for instance, to a slight misalignment of the sample or to the sample quality. The values of the spontaneous magnetization and the magnetization at saturation, $\approx 1\mu_B/Ce$, are consistent with those expected for a fundamental doublet Γ_7, while the observed anisotropy, though small, is not.

TABLE I. Values of the spontaneous and the saturated magnetization deduced from the experimental curves in the ferromagnetic phase along the three main axes of the cube. The last column reports the value of the magnetization at 4.2 K and 8 Tesla.

Axis	M_s (μ_B/Ce)	M_{sat} (μ_B/Ce)	M (8 T) (μ_B/Ce)
	100 mK	100 mK	4.2 K
[1 1 1]	0.91±0.02	1.05±0.02	0.96±0.02
[1 1 0]	0.76±0.02	1.01±0.02	0.90±0.02
[0 0 1]	0.59±0.02	0.98±0.02	0.90±0.02

At 4.2 K, the magnetization curves are characteristic of a paramagnetic behavior. Above 4 T, a weak but significant anisotropy of the magnetization is observed between the [111] direction and both the [001] and [110] axes. The values of the magnetization at 8 T are reported in table I. One remarks that at 4.2 K ($\approx 10\times T_C$) these values are very close to those of the magnetization at saturation in the ferromagnetic phase at 100 mK ($\approx T_C/4$).

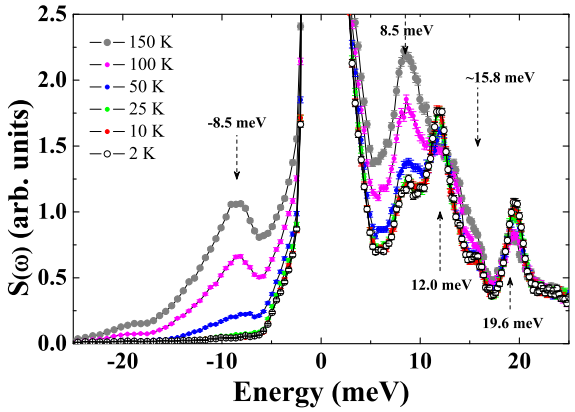

FIG. 6. (Color online) Thermal evolution of the inelastic scattering in $Ce_3Pt_{23}Si_{11}$ for incident neutrons of 36.7 meV. The spectra have been treated averaging out all the detectors.

V. NEUTRON STUDIES

All neutrons studies were carried out at the Institute Laue-Langevin (ILL) in Grenoble.

A. Neutron spectroscopy

The crystalline electric field (CEF) excitations were measured on a 7g sample by using the inelastic neutron scattering technique. Inelastic spectra were collected on the IN4 time-of-flight spectrometer for two incident wavelengths ($\lambda_i = 1.492$ Å and $\lambda_i = 2.22$ Å) which correspond to two different incident energies (E_i= 36.7 meV and E_i= 16.6 meV respectively) and two different instrument resolutions characterized by their full width at half maximum (FWHM) at the elastic position (FWHM = 1.65 meV and FWHM = 0.85 meV respectively). The measurements were conducted between 2 K and 150 K in order to discriminate between the magnetic and phonon excitations. The spectra were collected for scattering angles ranging from 13deg to 135deg, and were normalized respectively to incident flux and to a vanadium standard. The sample holder used for this experiment consisted of a thin aluminum foil, thus reducing the contribution of the empty cell to a minimum. The spectra were further grouped in different sections of the angle range in order to highlight either the energy dependence of the spectrum with maximum statistics (in that case all spectra are averaged out in a single spectrum), or the dependence on the scattering vector Q by grouping over a limited number of spectra. In the latter case, the scattering by magnetic excitations will be enhanced at low Q values (small angle sections) compared to phonons excitations which will be dominant at higher Q values.

Figure 6 shows the spectra collected between 2 and

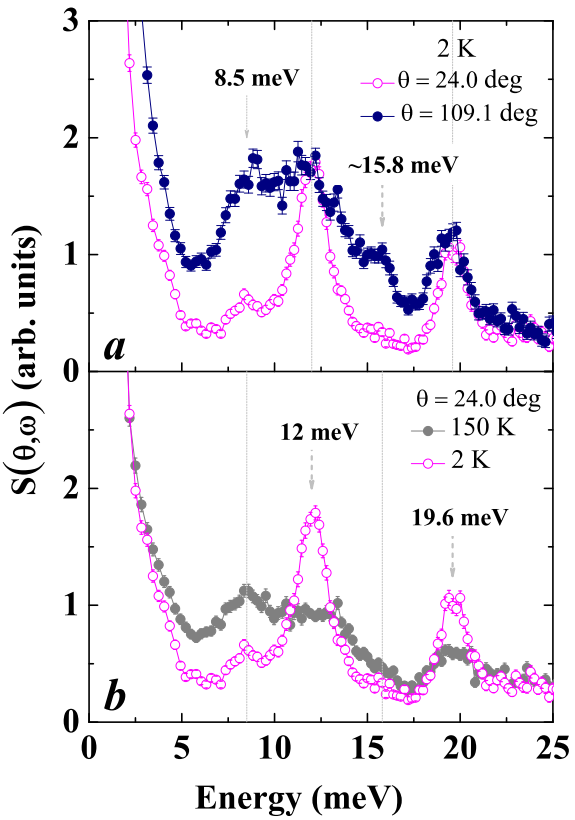

FIG. 7. (Color online) a) Inelastic intensities as function of the scattering angle at 2 K: open dots show the low angle detector averaging and full dots high angle detector averaging. b) Inelastic intensities as function of the temperature at low angle detector averaging: open dots show the spectrum at 2 K, full dots at 150 K.

150 K with an incident energy of 36.7 meV. These spectra have been treated averaging out all the detectors. At 2 K, three main inelastic structures are observed in the down-scattering processes at 8.5±0.2, 12±0.2 and 19.6±0.2 meV respectively, together with a small bump around 15.8 meV. When the temperature is increased, no change is observed in the spectra up to 50 K. From 50 K up to 150 K, the intensity of the structure at 8.5 meV strongly increases and its corresponding de-excitation is observed at -8.5 meV in the up-scattering process. Though smaller than the peak at 8.5 meV, an intensity increase in the down-scattering process is also observed around 15.8 meV, while both intensities at 12 and 19.6 meV decrease. The thermal evolution of the inelastic intensities is consistent with phonon excitations at 8.5 and 15.8 meV and magnetic excitations at 12 and 19.6 meV. To check the Q-dependence of the inelastic signal, the data have been re-treated by averaging out the spectra in 5 groups whose mean scattering angles θ are 24deg, 45.7deg, 66.3deg, 87.3deg and 109.1deg re-

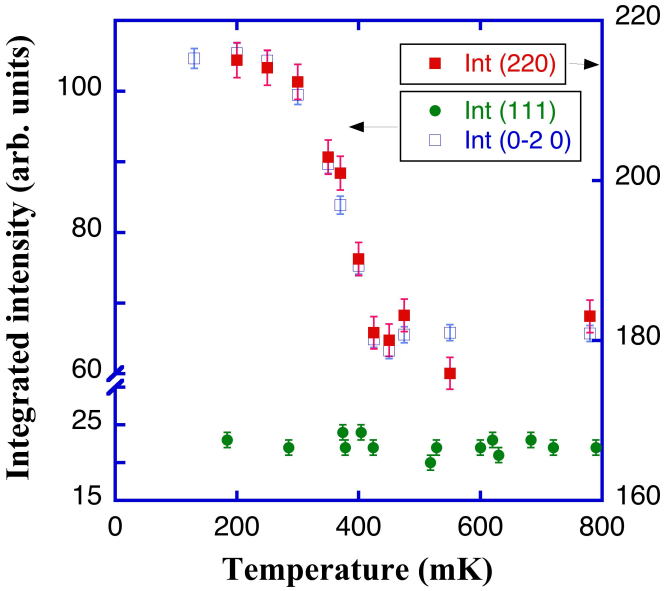

FIG. 8. (Color online) Thermal variation of the integrated intensity of the (220), (0$\bar{2}$0) and (111) reflexions. (Error bars are represented for each data point).

spectively. The evolution of the inelastic spectra with increasing scattering angles is a progressive increase of the intensity at 8.5 and 15.8 meV, together with a progressive decrease of the intensity at 12 and 19.6 meV. This is well illustrated by figure 7-a, which compares the inelastic spectra at θ_1=24deg and θ_5=109.1deg collected at 2 K. The figure 7-b compares for the same scattering angle, θ_1=24deg, the evolution of the intensities in the down-scattering processes between 2 and 150 K. It confirms the decrease at high temperature of the intensity at 12 and 19.6 meV in agreement with figure 6.

It turns out that two inelastic excitations, E_1 = 12 meV (139.3 K) and E_2 = 19.6 meV (227.5 K), with a magnetic-like behavior are observed in the paramagnetic phase of $Ce_3Pt_{23}Si_{11}$ while only one Γ_7-Γ_8 CEF transition is expected for this cubic compound. The existence of a second excitation could be due to transitions towards the excited $J' = 7/2$ multiplet. Generally, such a behavior is observed in very anomalous Ce compounds, like for instance in $CeRh_3B_2$, and the energies of the transitions are one order of magnitude higher than those observed here.[12] A first observation of two CEF excitations in a cubic Ce compound has been previously reported in $CeAl_2$.[13] It was interpreted by Thalmeier and Fulde (Ref. 14) and latter on by Thalmeier (Ref. 15) in terms of an unusual magneto-elastic coupling that gives rise to a bounding state between the CEF and low-lying vibronic states. This will be discussed later.

B. Neutron diffraction

Neutron diffraction experiments were performed on $Ce_3Pt_{23}Si_{11}$ single crystal using the four-circle diffractometer D10 at ILL with a neutron wavelength λ = 2.36 Å. The very low temperature T = 140 mK was reached thanks to the unique four-circle dilution cryostat available on D10. A set of 581 nuclear reflections were collected in the paramagnetic phase at T = 800 mK. However due to the high symmetry of the nuclear structure, this set reduces to only 34 independent reflections. The refinements of the integrated intensities were carried out using the FullProf program[16] and the CCSL software[17]. A good agreement between observation and calculation is obtained with the cubic $Fm\bar{3}m$ space group giving to RF2 and RF factors of 11.6% and 6.7% respectively. At low temperature T = 140 mK, no additional reflection is observed, however, the intensity of some nuclear peaks increases below T_C = 440 mK. The fcc-lattice translations are also translations for the magnetic structure, the magnetic propagation vector is then $\vec{k}$=[000]. A set of 203 reflections were collected at T = 140 mK. Figure 8 shows the temperature dependence of the 220 0$\bar{2}$0 and 111 reflections. In the fcc structure ($Fm\bar{3}m$), the magnetic Ce atoms occupy the 24d site. They are located at the positions (0.25 0 0.25), (-0.25 0 0.25), (0 0.25 0.25), (0 -0.25 025), (0.25 0.25 0), (-0.25 0.25 0) and numbered as Ce_1, Ce_2, Ce_3, Ce_4, Ce_5 and Ce_6 respectively. As shown on the figure, the magnetic contribution is observed only on the top of nuclear reflections of the fcc lattice with hkl all even, while no contribution is observed for reflections with odd indices. The non-observation of magnetic contribution on reflections with odd indices, is a strong constrain on the magnetic coupling and leads to a ferromagnetic coupling between Ce_1 and Ce_2, Ce_3 and Ce_4, Ce_5 and Ce_6 respectively. Group theory analysis was used to determine the magnetic configurations of Ce atoms in the $Fm\bar{3}m$ space group. The propagation vector being $\vec{k} = 0$, the relevant irreducible representations (IR) of the magnetic structure are those of the point group $m\bar{3}m$. There are ten irreducible representations labeled Γ_1, Γ_2, Γ_3, Γ_4, of dimension 1, Γ_5, Γ_6 of dimension 2, Γ_7, Γ_8, Γ_9 and Γ_{10} of dimension 3. The reduction of the magnetic or induction representation of the site 24d gives Γ_{24d}= Γ_3+Γ_6+2Γ_8+3Γ_{10}. The basis vectors which span the space of a given irreducible representation are obtained by the projection operator technique.[18,19] The only non-zero basis vectors of the site 24d are those of Γ_3, Γ_6 , Γ_8 and Γ_{10}. The basis vectors of Γ_3, Γ_6, Γ_8 describe antiferromagnetic arrangements, while those of Γ_{10} correspond to a ferromagnetic arrangement. The basis vectors for Γ_{10} are written below:

Basis vector ψ_1:

$V_{11}=(M_{Ce1}+M_{Ce2})_Z$

$V_{21}=(M_{Ce3}+M_{Ce4}+M_{Ce5}+M_{Ce6})_Z$

$V_{31}=(M_{Ce3}-M_{Ce4})_Y+(M_{Ce1}-M_{Ce2})_X$

Basis vector ψ_2:

$V_{12}=(M_{Ce3}+M_{Ce4})_X$

V_{22}=(M_{Ce1}+M_{Ce2}+M_{Ce5}+M_{Ce6})$_X$
V_{32}=(M_{Ce1}-M_{Ce2})$_Y$+(M_{Ce5}-M_{Ce6})$_Z$
Basis vector ψ_3:
V_{13}=(M_{Ce5}+M_{Ce6})$_Y$
V_{23}=(M_{Ce1}+M_{Ce2}+M_{Ce3}+M_{Ce4})$_Y$
V_{33}=(M_{Ce1}-M_{Ce2})$_X$+(M_{Ce3}-M_{Ce4})$_Z$

The basis vectors ψ_1 , ψ_2 and ψ_3 describe a ferromagnetic arrangement along [100], [010] and [001] axis respectively, while a combination of the three basis vectors leads to a ferromagnetic arrangement along the [111] direction.

Due to cubic symmetry, the averaged observed integrated intensities, lead to the same magnetic intensities when the magnetic moment direction is along the principal axis. The refinement of the magnetic moment from the measured intensity in the ordered state leads to a value of 1.2(2) μ_B per cerium ion, which is close to that deduced from the magnetization measurements. The scaling factor and the structural parameters used in the refinement are those deduced from the refinement in the paramagnetic phase.

VI. DISCUSSION

Magnetic measurements in the ferromagnetic phase of $Ce_3Pt_{23}Si_{11}$ show that a weak but significant anisotropy exists with an easy magnetization axis along the three-fold axes of the cube. As said above, the observation of a magnetic anisotropy is not consistent with a Γ_7 doublet CEF fundamental. On the other hand, the spontaneous magnetization along the [111] axis, 0.91±0.02 μ_B/Ce, is closer to the expected value for the Γ_7 CEF ground state than for the Γ_8. An other intriguing point is the observation of two inelastic lines of magnetic origin in the neutron spectroscopy spectra, while neutron diffraction experiments confirm that, within the experimental accuracy, the crystallographic structure remains cubic at least down to 800 mK. A similar feature has been reported for the cubic Kondo compound $CeAl_2$ and interpreted by the existence of a very unusual and strong magneto-elastic coupling that leads to a bound state between the CEF and low-lying vibronic states.[13–15] In Kondo systems one may expect a non negligible magneto-elastic coupling between an appreciable extended $4f$ orbital and the lattice degrees of freedom, via the hybridization of the $4f$ electron and the conduction band. However, the existence of a CEF-phonon bound state requires very peculiar conditions. In a neutron scattering process, both magnetic and phonon scattering are present but their contributions can be separated in most cases because they have a different behavior as function of the momentum transfer. In $CeAl_2$, the CEF-phonon bound state exists because of very peculiar conditions *i.e.* low-lying phonon branches of the Ce sub-lattice peaking at the same energy than the CEF excitations. This is why such an effect has been reported for only very few compounds, $YbPO_4$ and $CeCu_2$, besides $CeAl_2$.[20] At the present stage of the study, there is no experimental evidence of anomalous magneto-elastic effects in $Ce_3Pt_{23}Si_{11}$, except may be the fact that in the neutron scattering spectra the phonon peak intensities start increasing and the CEF peak intensities start decreasing simultaneously only above 50 K (see Fig. 6). The bulk heat capacity of $Ce_3Pt_{23}Si_{11}$ shows a standard behavior in the paramagnetic phase, exactly similar to that of $La_3Pt_{23}Si_{11}$ with the same Debye temperature. Due to the stoichiometry, the Ce or La ions are highly diluted in a matrix made up almost entirely of Pt. Thus the contribution of the Pt sub-lattice to the low-lying phonon spectrum can hardly be neglected in $Ce_3Pt_{23}Si_{11}$ or $La_3Pt_{23}Si_{11}$ contrary to $CeAl_2$.

The interpretation of the two inelastic lines in the scattering spectrum of $CeAl_2$ by a CEF-phonon bound state is strongly supported by the fact that the CEF excited state, the Γ_8 quadruplet, can be split by the magnon-phonon coupling during the scattering process. A similar splitting for the Γ_7 excited state is not possible. We tentatively analyzed the magnetic measurements in $Ce_3Pt_{23}Si_{11}$ within the CEF formalism in order to deduce the CEF ground state. For Ce^{3+} ions in cubic symmetry only fourth degree terms are effective in the CEF Hamiltonian, thus only the parameter W = $\pm E_{CEF}/6$ has to be considered in the Lea, Leask and Wolf parametrization.[21] Assuming a CEF splitting, $E_{CEF} \approx (E_1 + E_2)/2 \approx$183 K leads to W = ±30.5 K. A positive (negative) value of W selects a Γ_7 (Γ_8) as CEF ground state. In rare earth compounds, quadrupolar and/or magneto-elastic interactions may strongly perturb the magnetic properties and in some cases may change the easy axis. We thus included the quadrupolar interactions in the calculations besides the bilinear Heisenberg-type exchange.[22] The basic Hamiltonian given by the sum of the CEF, exchange, Zeeman and total quadrupolar Hamiltonians, is diagonalized. The bilinear exchange (n) and the total quadrupolar coupling ($G_{\gamma,\epsilon}$) that account for both the magneto-elastic and purely quadrupolar couplings are treated within the mean-field approximation. The bilinear exchange parameter, n = θ_p/C (θ_p is the paramagnetic Curie temperature and C the Curie constant), has been determined for each ground state as the value calculated for the inverse of the susceptibility at T_C = 440 mK: n = 1.265 T/μ_B and 0.492 T/μ_B for a Γ_7 and a Γ_8 ground state, respectively. A first series of calculations has been performed taking into account only the bilinear exchange. Figure 3 shows the thermal variation of the inverse of the susceptibility calculated with W = ±30.5 K and compares it to the calculations performed with W = ±23 K (E_1/6) and W = ±38 K (E_2/6) respectively. The best consistency between calculations and experimental data is obtained for the negative values of W *i.e.* for a Γ_8 quadruplet ground state. In figure 9, the calculated magnetization curves with W = ±30.5 K are compared with the experimental curves obtained at 4.2 K along the three main axes of the cube.

At first glance, the calculations give again a much better agreement for the Γ_8 ground state. In the low field region up to 2 T, the agreement is very good for the three directions with no anisotropy consistently with the susceptibility measurements. Under higher fields, the calculations predict a weak anisotropy with a larger magnetization along the fourfold [001] axis. Actually, as shown in figure 5, the experimental anisotropy of the magnetization is much weaker and would favor the [111] axis. Systematically, the calculated values are larger than the experimental ones for each axis. The discrepancy between calculations and experimental data is larger along the fourfold axis. We note that calculations, not reported here, performed with W = ±23 K and ±38 K lead to exactly the same behavior and same values for the magnetization. Also it is worth noting that the calculations of the Schottky anomaly in the heat capacity lead to a contribution three times smaller for a Γ_8 than for a Γ_7 ground state, regardless of the value of W. Thus a Γ_8 ground state would be in a better agreement with the experimental heat capacity reported in figure 1, which shows no anomaly.

We tried to reduce the discrepancy along the [001] axis by introducing quadrupolar couplings. Along this axis, only the tetragonal lowering symmetry mode (γ mode) has to be considered. The magnetization can be reduced only for negative quadrupolar parameters. The best result is obtained with G_γ = -65 mK that leads to a reduction of about 16% for the magnetization along the [001] axis. For values of G_γ<-65 mK the calculations become unstable. As shown in figure 10 introducing a negative quadrupolar coupling leads to a pronounced reduction of the magnetization in the ferromagnetic phase. Though the calculated values appear in better agreement with the experimental data, calculations still predict a fourfold easy axis. In both, the paramagnetic and ferromagnetic phases, the quadrupolar coupling has no effect for a Γ_7 fundamental no matter the value and the sign of G_γ.

Within the conventional formalism used here, the magnetic properties in the paramagnetic phase and under low magnetic fields: susceptibility and magnetization curves, are consistent with a cubic ground state Γ_8. However, within the same formalism, a Γ_8 ground state leads inevitably to a fourfold easy axis contrarily to the observed anisotropy in the ferromagnetic phase. Also group theory analysis predicts a ferromagnetic arrangement along the threefold [111] axis. The results would suggest sizable negative quadrupolar or magneto-elastic couplings in $Ce_3Pt_{23}Si_{11}$. It is quite surprising that non negligible antiferroquadrupolar couplings could exist in a ferromagnetic compound. On the other hand, the apparent stability of the cubic lattice makes questionable the existence of strong magneto-elastic couplings. In any case, further studies of the magneto-elastic properties, such as elastic constants, magneto-striction and third-order susceptibility measurements are necessary to support the existence of such strong couplings. Assuming a Γ_8 ground state,

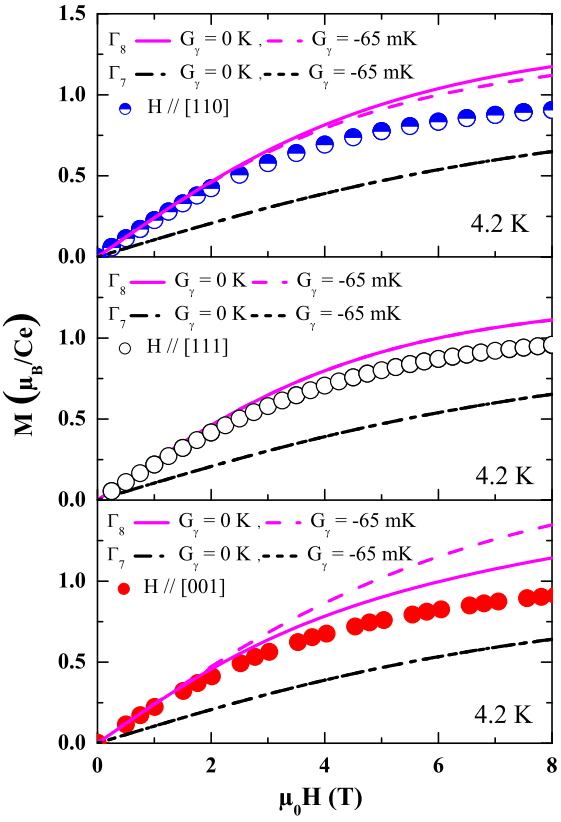

FIG. 9. (Color online) Comparison between calculated and experimental magnetization curves at 4.2 K along the three main axes of the cube. The Hamiltonian given by the sum of the CEF, exchange, Zeeman and total quadrupolar Hamiltonians, is diagonalized. The couplings: the spin Heisenberg-type exchange and the total quadrupolar coupling, are treated within the mean-field approximation. The calculations have been performed for two values of the CEF parameter W = ±30.5 K. W = -30.5 K selects the Γ_8 ground state and the exchange constant deduced from the calculated susceptibility is n = 0.492 T/μ_B. In the figure, the full and dashed lines represent the calculations with a total quadrupolar constant G_γ = 0 and -65 mK respectively. For W = +30.5 K the ground state is the Γ_7 doublet and the exchange constant is n = 1.265 T/μ_B. In the figure the dash dot and short dash lines represent the calculations with a total quadrupolar constant G_γ = 0 and -65 mK respectively.

the two inelastic lines observed in the neutron spectra cannot be accounted for, unless a strong lattice distortion splits the quadruplet into two doublets. As said above this is not observed by static experiments. Moreover the Thalmeier model can not apply in case of a Γ_8 ground state because the excited doublet Γ_7 cannot be split. The present analysis performed within a static cubic symmetry fails in explaining coherently the different properties and experimental observations in $Ce_3Pt_{23}Si_{11}$. A last possibility that could be considered is the split-

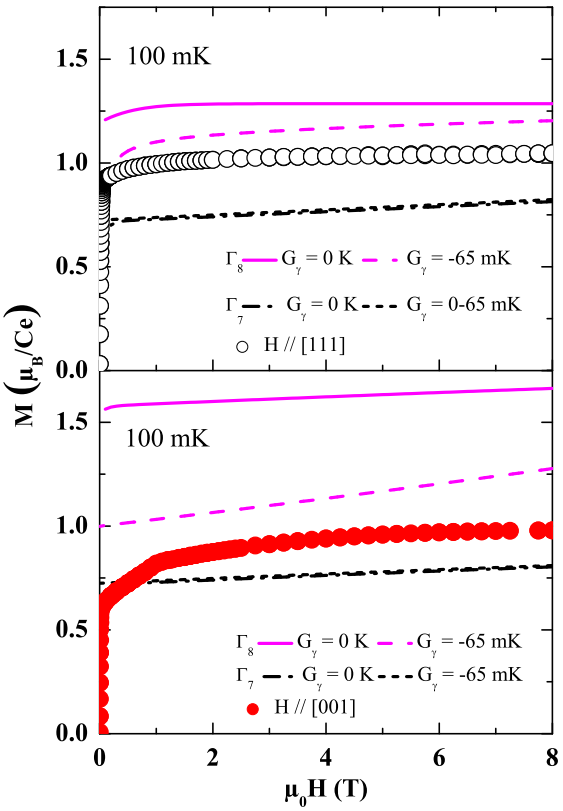

FIG. 10. (Color online) Calculated (lines)and experimental (dots) magnetization curves in the ferromagnetic phase along the fourfold and three fold axes. The full and dashed lines represent the calculations for a Γ_8 ground state with a bilinear exchange constant n = 0.492 T/μ_B and a total quadrupolar constant G_γ = 0 and -65 mK respectively. The dash dot and short dash lines represent the calculations for a Γ_7 fundamental with n = 1.265 T/μ_B and a total quadrupolar constant G_γ = 0 and -65 mK respectively.

ting of the Γ_8 ground state via a Dynamical Jahn-Teller effect, in which case the apparent crystal symmetry remains cubic.[23] Further experimental work is required to explore this hypothesis.

VII. CONCLUSIONS

A large panel of experimental techniques has been used to study the physical properties of $Ce_3Pt_{23}Si_{11}$. Heat capacity and electrical resistivity are in agreement with a good metal behavior. In the paramagnetic phase, the magnetic susceptibility presents a thermal variation fully consistent with a normal trivalent cerium ion. In the same paramagnetic phase however the neutron spectroscopy reveals very unusual inelastic spectra with the existence of two magnetic excitations in this cubic cerium compound. Attempts to determine the CEF ground state within the CEF formalism let suppose that a Γ_8 quadruplet ground state would be more consistent with the magnetic properties at least in low fields. In the ferromagnetic phase however, the anisotropy of the spontaneous magnetization is no more consistent with a quadruplet ground state. Also, along the three high symmetry axes, the magnetization under high field tends to almost the same value, $\approx 1\ \mu_B$/Ce. This value is smaller than the expected 1.571 μ_B/Ce for the Γ_8 ground state and the apparent isotropy let suppose a splitting of the quadruplet into two doublets. This may be ascribed to a Dynamical Jahn-Teller effect.

ACKNOWLEDGMENTS

Authors are indebted to A.P. Murani for fruitful discussions and valuable help. We greatly acknowledge the technical assistance of A. Hadj-Azzem, J. Balay, D. Dufeu, E. Eyraud and P. Lachkar from the Néel Institute.

* christine.opagiste@grenoble.cnrs.fr

[1] A. I. Tursina, A. V. Gribanov, Y. D. Seropegin, K. V. Kuyukov, and O. I. Bodak, J. Alloys Compd., **347**, 121 (2002).

[2] A. V. Gribanov, Y. D. Seropegin, A. I. Tursina, O. I. Bodak, P. Rogl, and H. Noel, J. Alloys Compd., **383**, 286 (2004).

[3] K. Nakatsuji, A. Sumiyama, Y. Oda, T. Yasuda, R. Settai, and Y. Onuki, J. Phys. Soc. Jpn., **75**, 084717 (2006).

[4] E. Scheidt, F. Mayr, G. Eickerling, P. Rogl, and E. Bauer, J. Phys.: Condens. Matter, **17**, L121 (2005).

[5] J. S. Kim, D. J. Mixson, D. J. Burnette, T. Jones, P. Kumar, B. Andraka, G. R. Stewart, V. Craciun, W. Acree, H. Q. Yuan, D. Vandervelde, and M. B. Salamon, Phys. Rev. B, **71**, 212505 (2005).

[6] I. Bonalde, R. L. Ribeiro, W. Bramer-Escamilla, C. Rojas, E. Bauer, A. Prokofiev, Y. Haga, T. Yasuda, and Y. Onuki, New J. Phys., **11**, 055054 (2009).

[7] E. Bauer, H. Kaldarar, A. Prokofiev, E. Royanian, A. Amato, J. Sereni, W. Bramer-Escamilla, and I. Bonalde, J. Phys. Soc. Jpn., **76**, 051009 (2007).

[8] C. Opagiste, C. Paulsen, E. Lhotel, P. Rodiere, R.-M. Galera, P. Bordet, and P. Lejay, J. Magn. Magn. Mater., **321**, 613 (2009).

[9] D. C. Kundaliya and S. K. Malik, Phys. Rev. B, **67**, 132411 (2003).

[10] M. Bouvier, P. Lethuillier, and D. Schmitt, Phys. Rev. B, **43**, 13137 (1991).

[11] A. Arrott, Phys. Rev., **108**, 1394 (1957).

[12] F. Givord, J.-X. Boucherle, A. P. Murani, R. Bewley, R.-M. Galéra, and P. Lejay, J. Phys.: Condensed Matter, **19**,

506210 (2007).
[13] M. Loewenhaupt, B. D. Rainford, and F. Steglich, Phys. Rev. Lett., **42**, 1709 (1979).
[14] P. Thalmeier and P. Fulde, Phys. Rev. Lett., **49**, 1588 (1982).
[15] P. Thalmeier, J. Phys. C: Solid State Phys., **17**, 4153 (1984).
[16] FullProf, http://www.ill.eu/sites/fullprof/.
[17] J. C. Matthewman, P. Thompson, and P. Brown, J. Appl. Cryst., **15**, 167 (1982).
[18] G. Y. Lyubarskii, *The Application of Group Theory in Physics* (Pergamon, Oxford, 1960).
[19] V. Heine, *Group Theory in Quantum Mechanics*, Appendix K (Pergamon, Oxford, 1960).
[20] M. Loewenhaupt and U. Witte, J. Phys.: Condens. Matter, **15**, S519 (2003).
[21] K. Lea, M. Leask, and W. Wolf, J. Phys. Chem. Solids, **23**, 1381 (1962).
[22] P. Morin and D. Schmitt, *Quadrupolar interactions and magneto-elastic effects in rare earth intermetallic compounds*, Ferromagnetic Materials, Vol. 5 (Elsevier Science, 1990).
[23] A. Abragam and M. H. L. Pryce, Proceedings of the Physical Society. Section A, **63**, 409 (1950).